iScience

CellPress
OPEN ACCESS

Article

The alarmin IL-33 exacerbates pulmonary inflammation and immune dysfunction in SARS-CoV-2 infection

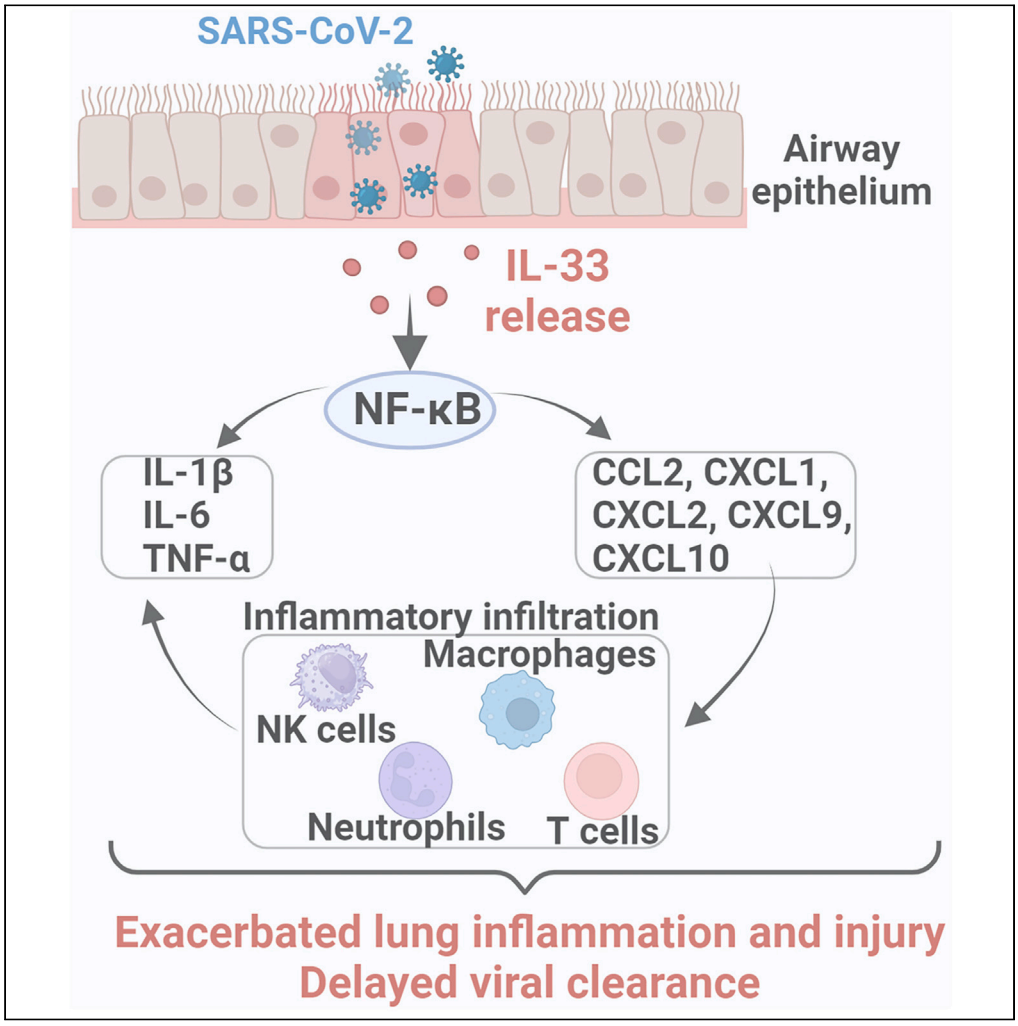

Hui Wang, Yashoda M. Hosakote, Paul J. Boor, ..., Lynn Soong, Jiaren Sun, Yuejin Liang

yu2liang@utmb.edu

Highlights

SARS-CoV-2 infection triggers IL-33 expression in both patients and mouse models

IL-33 activates NF-κB signals and enhances lung inflammatory responses

Deficiency of IL-33 leads to reduced pulmonary pathology

Wang et al., iScience 27, 110117
June 21, 2024
https://doi.org/10.1016/j.isci.2024.110117

iScience

CellPress
OPEN ACCESS

Article

The alarmin IL-33 exacerbates pulmonary inflammation and immune dysfunction in SARS-CoV-2 infection

Hui Wang,[1,2] Yashoda M. Hosakote,[2,3] Paul J. Boor,[1] Jun Yang,[4] Yuanyi Zhang,[5] Xiaoying Yu,[5] Casey Gonzales,[1] Corri B. Levine,[4] Susan McLellan,[4] Nicole Cloutier,[4] Xuping Xie,[6] Pei-Yong Shi,[6] Ping Ren,[1] Haitao Hu,[3] Keer Sun,[3] Lynn Soong,[1,3] Jiaren Sun,[1,3] and Yuejin Liang[2,3,7,*]

SUMMARY

Dysregulated host immune responses contribute to disease severity and worsened prognosis in COVID-19 infection and the underlying mechanisms are not fully understood. In this study, we observed that IL-33, a damage-associated molecular pattern molecule, is significantly increased in COVID-19 patients and in SARS-CoV-2-infected mice. Using IL-33$^{-/-}$ mice, we demonstrated that IL-33 deficiency resulted in significant decreases in bodyweight loss, tissue viral burdens, and lung pathology. These improved outcomes in IL-33$^{-/-}$ mice also correlated with a reduction in innate immune cell infiltrates, i.e., neutrophils, macrophages, natural killer cells, and activated T cells in inflamed lungs. Lung RNA-seq results revealed that IL-33 signaling enhances activation of inflammatory pathways, including interferon signaling, pathogen phagocytosis, macrophage activation, and cytokine/chemokine signals. Overall, these findings demonstrate that the alarmin IL-33 plays a pathogenic role in SARS-CoV-2 infection and provides new insights that will inform the development of effective therapeutic strategies for COVID-19.

INTRODUCTION

COVID-19 is caused by severe acute respiratory syndrome coronavirus 2 (SARS-CoV-2) infection and is known to cause a spectrum of symptoms in humans that range from asymptomatic to severe multi-organ failure and death.[1] Notably, COVID-19 infection can result in pathological changes in the lungs and various extrapulmonary complications. Disease severity is closely tied to activation of inflammatory responses that are predominantly considered to be part of a dysregulated innate immune reaction. This dysregulated innate immune reaction is marked by a delayed interferon response and vigorous viral replication that result in cytokine storms (CS) and inflammation-induced tissue damage, especially in the lungs.[2–4] Although the global distribution of SARS-CoV-2 vaccines has successfully curtailed severe disease and fatalities, continuous viral evolution has raised concerns regarding the effectiveness of current vaccines.[5] Despite our increased understanding of SARS-CoV-2, the host factors that contribute to a dysregulated immune response and excessive pulmonary inflammation are not fully understood. Therefore, a better understanding of the molecular mechanisms that underlie dysregulated immune responses in SARS-CoV-2 infections will be instrumental in providing key evidence to inform the development of innovative therapeutic strategies to treat COVID-19.

Emerging data have revealed that both the innate and adaptive immune responses are not only involved in protection from SARS-CoV-2 but also in the pathological changes of severe COVID-19. In particular, innate immune cells, including neutrophils, inflammatory monocytes, and activated macrophages, trigger CS in severe COVID-19 through overproduction of several inflammatory cytokines (IL-1β, IL-6, IL-12, IL-17, IL-18, IFN-γ, TNF-α, G-CSF, and GM-CSF).[6] Therefore, therapeutics aimed at controlling hyperinflammatory responses could reduce disease severity in COVID-19 patients. Unfortunately, significant efforts in clinical trials revealed that the efficacy of immune modulators (e.g., neutralizing IL-1, IL-6, and GM-CSF) has not met expectations.[7–10] However, identification of key molecules that regulate hyperinflammation during SARS-CoV-2 infection remains critically important. Damage-associated molecular patterns (DAMPs) are endogenous danger molecules released from damaged or stressed cells. DAMPs have the ability to enhance both innate and adaptive immune responses, which amplify inflammation and cause additional damage to tissues and cells.[11] Interleukin-33 (IL-33) is a DAMP molecule that is highly expressed in epithelial and endothelial cells and significantly contributes to inflammation in airway diseases.[12] IL-33 possesses opposing functions in that it can

[1]Department of Pathology, University of Texas Medical Branch, Galveston, TX 77555, USA
[2]Institute for Human Infections and Immunity, University of Texas Medical Branch, Galveston, TX 77555, USA
[3]Department of Microbiology and Immunology, University of Texas Medical Branch, Galveston, TX 77555, USA
[4]Department of Internal Medicine, Division of Infectious Diseases, University of Texas Medical Branch, Galveston, TX 77555, USA
[5]Department of Biostatistics and Data Science, the University of Texas Medical Branch, Galveston, TX 77555, USA
[6]Department of Biochemistry and Molecular Biology, University of Texas Medical Branch, Galveston, TX 77555, USA
[7]Lead contact
*Correspondence: yu2liang@utmb.edu
https://doi.org/10.1016/j.isci.2024.110117

trigger type 1 or type 2 immune responses depending on the disease and the time after infection.[13–16] This dual role enables IL-33 to contribute to both immune activation and tissue repair processes.[17–19] Recent clinical studies have provided evidence of a positive correlation between high IL-33 expression and increased COVID-19 severity. One observational study showed increased IL-33 expression in peripheral blood mononuclear cells (PBMCs) from SARS-CoV-2 seropositive individuals, and IL-33 also correlated with $CD4^+$ T cell activation in PBMCs from convalescent individuals.[20] Increased serum IL-33 levels were also found to be associated with increased COVID-19 disease severity, suggesting that IL-33 could be a useful indicator for prognosis in patients.[21,22] We previously reported that SARS-CoV-2 infection upregulated IL-33 expression in human epithelial cell culture,[15] indicating that IL-33 may contribute to pulmonary inflammation and pathology in COVID-19.[23,24] However, the precise role of IL-33 and the mechanisms that underlie IL-33 function(s) during SARS-CoV-2 infection remain unknown.

In the present study, we identified correlations between IL-33 levels in plasma and naso-/oro-pharyngeal swab samples and the severity of COVID-19 in patients. We also demonstrated that IL-33 is necessary for lung inflammation and damage in a mouse-adapted SARS-CoV-2, IL-33-deficient mouse model. Bulk RNA-seq analysis of lung tissues revealed that IL-33 is involved in multiple facets of immune activity, including infiltration of inflammatory cells, leukocyte maturation, interferon signaling, and activation of the NF-κB pathway. These findings indicate that IL-33 could be a promising target for potential therapeutic interventions in the treatment of COVID-19.

RESULTS

SARS-CoV-2 infection induces IL-33 expression and inflammatory cytokine release

First, we quantified IL-33 levels in plasma and nasopharyngeal swab samples from COVID-19-positive patients. As shown in Figure 1A, IL-33 levels in the nasopharynx positively correlated with disease severity. Patients with moderate to severe symptoms had significantly higher plasma IL-33 levels compared to healthy donors and patients with mild symptoms. Patients with critical symptoms also exhibited an increased plasma IL-33, although this correlation was not statistically significant. These results suggest that IL-33, especially in the nasopharynx, might be a promising biomarker for predicting COVID-19 severity.

To determine whether SARS-CoV-2 infection induces IL-33 expression in mice, we intranasally (i.n.) infected C57BL/6j (B6) mice with a mouse-adapted SARS-CoV-2 virus CMA3p20.[25] Mice were monitored after infection and serum and lung tissue were collected on D2 and D4 post-infection for RNA-seq and Bio-Plex analysis. We determined that the pulmonary viral burden peaked at day 2 (D2) and subsequently decreased at D4 (Figure S1A). Increased viral burden and upregulated IL-33 levels in lung tissue were also observed in Delta strain infected K18-hACE2 mice compared to control (Figures S1B and S1C). The transcript levels of proinflammatory chemokines (*Ccl2*, *Cxcl1*, and *Cxcl2*) and cytokines (*Ifnb*, *Ifng*, *Il6*, *Tnf*, and *Csf1*) were significantly increased in lung tissue of C57BL/6j mice at D2 but were similar to mock-treated levels at D4 (Figure 1B). *Il10* and *Il13* expression levels were increased at D4 compared to control, while no significant change in *Il4* expression was observed during infection (Figure 1B). Serum Bio-Plex data demonstrated that cytokines (IL-5, IL-6, IL-12p40, and G-CSF) and chemokines (CXCL1, CCL2, and CCL5) were significantly upregulated at D2, while levels of IL-12p40 and CCL5 remained high through D4 (Figures 1C and S2). As shown in Figure 1D, the transcript and protein levels of IL-33 in lung tissue were increased at D2 and D4 compared to the mock group. Collectively, our data indicate that SARS-CoV-2 infection triggers the release of DAMP molecule IL-33 and induces inflammatory cytokine release in mice.

Deficiency of IL-33 alleviates inflammatory infiltration, reduces cytokine production, and decreases viral loads in mice

To evaluate the role of endogenous IL-33 in the pathogenesis of SARS-CoV-2 infection, wild type (WT) and $IL\text{-}33^{-/-}$ mice were infected with the mouse adapted SARS-CoV-2 virus CMA3p20. We found that $IL\text{-}33^{-/-}$ mice exhibited less bodyweight loss at D2 and D3 and had lower viral burden in the lungs at D4 as compared to WT mice (Figures 2A and 2B). Histological examination of the lungs showed reduced peribronchiolar PMN infiltration and reduced intrabronchial mucus and cell debris in the lungs of $IL\text{-}33^{-/-}$ mice at D2 compared to WT mice. This finding indicates that mice lacking IL-33 experienced less lung damage than WT mice. At D4, histological change in $IL\text{-}33^{-/-}$ mice consisted of mild inflammation with collections of mucus and epithelial cells that were noted to be undergoing regeneration (Figure 2C). We also performed multicolor flow cytometric analysis of infiltrated immune cells in the lungs and the gating strategy is depicted in Figure 2D. Our data showed significantly decreased pulmonary infiltration of neutrophils, activated NK cells, and macrophages on D2 in $IL\text{-}33^{-/-}$ mice (Figure 2E). IL-33 deficiency also resulted in decreased numbers of activated $CD4^+$ and $CD8^+$ T cells, but not γδ T cells, in the lungs at D4 (Figure 2E). Next, we examined the levels of inflammatory cytokines and chemokines in serum (Figure 2F) and observed a significant reduction in IL-5 and IL-6 at D2 in $IL\text{-}33^{-/-}$ mice compared to WT mice. Additionally, IL-12p40, CXCL1, CCL2, and granulocyte colony-stimulating factor (G-CSF) levels were significantly decreased in $IL\text{-}33^{-/-}$ mice at D2. CCL11 was found to be reduced in $IL\text{-}33^{-/-}$ mice only at D4. Interestingly, $IL\text{-}33^{-/-}$ mice had higher serum IFN-γ levels at D2 compared to WT mice. Altogether, our results demonstrate that endogenous IL-33 contributes to pulmonary inflammatory responses and systemic cytokine production in mice following SARS-CoV-2 infection.

Exogenous IL-33 exacerbates lung inflammation in SARS-CoV-2-infected mice

To determine whether exogenous IL-33 would exacerbate the inflammatory response during SARS-CoV-2 infection, we i.n. treated mice with recombinant IL-33 (rIL-33) at D1 and D3, respectively (Figure 3A). rIL-33 treatment resulted in more bodyweight loss at D3 compared to the control group (Figure 3B). No significant changes in body weight were observed in uninfected mice with or without rIL-33 treatment (Figure 3B). In addition, rIL-33 treatment delayed viral clearance at D4 (Figure 3C), as evidenced by higher viral loads in rIL-33-treated mice compared to control mice (mean ± SD: 5602 ± 2670 vs. 1365 ± 462 copy numbers/ng lung RNA). Histological analysis of lung tissue showed

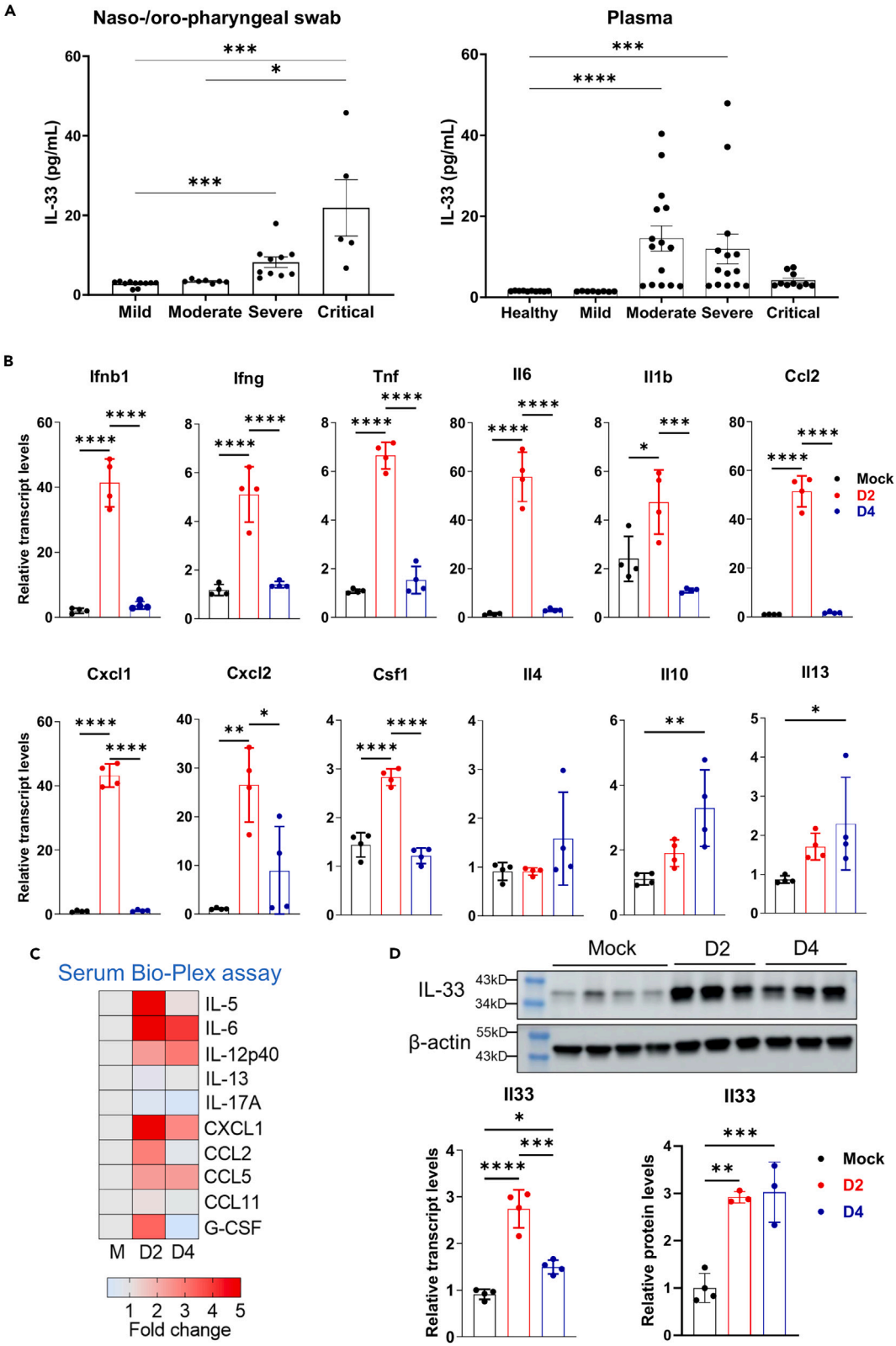
A
Naso-/oro-pharyngeal swab
IL-33 (pg/mL)
Mild
Moderate
Severe
Critical
Plasma
Healthy
B
Ifnb1
Ifng
Tnf
Il6
Il1b
Ccl2
Cxcl1
Cxcl2
Csf1
Il4
Il10
Il13
Relative transcript levels
Mock
D2
D4
C
Serum Bio-Plex assay
IL-5
IL-6
IL-12p40
IL-13
IL-17A
CXCL1
CCL2
CCL5
CCL11
G-CSF
M D2 D4
1 2 3 4 5
Fold change
D
Mock
D2
D4
IL-33
43kD
34kD
β-actin
55kD
43kD
Il33
Relative transcript levels
Relative protein levels

Figure 1. SARS-CoV-2 infection leads to increased IL-33 levels and pulmonary inflammation

(A) IL-33 levels in human plasma and naso-/oro-pharyngeal swabs were higher in COVID-19 patients. Patient demographics, clinical status, and numbers in each group are shown in Table S2.

(B) B6 mice ($n = 4$/group) were i.n. inoculated intranasally (i.n.) with 5×10^5 PFU SARS-CoV-2 CMA3p20. Lung tissues and sera were harvested at D2 and D4. Mock mice received an inoculation of virus-culture medium. Relative fold changes in the gene expression of cytokines (*Ifnb1*, *Ifng*, *Tnf*, *Il6*, *Il1b*, *Il10*, and *Csf1*) and chemokines (*Cxcl1*, *Cxcl2*, and *Ccl2*) within lung tissues were determined by RT-qPCR.

(C) Serum cytokine and chemokine levels were measured by Bio-Plex assay. The heatmap was generated using fold-changes which were calculated in comparison to mock samples.

(D) Lung IL-33 transcript and protein levels were determined by RT-qPCR and western blot, respectively. Human data were analyzed by nonparametric analysis, followed by Dunn's multiple comparisons test. Mouse bodyweight change was analyzed using repeated measures two-way ANOVA. Pairwise comparisons were performed by Tukey's multiple comparisons test at each time point. All other mouse data were analyzed by one-way ANOVA, followed by Tukey's multiple comparison test. The results are presented as the mean ± SD, and the animal experiment was performed twice independently. Statistically significant values are denoted as $*p < 0.05$, $**p < 0.01$, $***p < 0.001$, and $****p < 0.0001$.

focally infiltrating immune cells filling the alveolar spaces (lung consolidation) and appeared worse in rIL-33-treated animals (Figure 3D). By D4, immune cell infiltration seemed to partially resolve when areas of fibrosis and bronchial epithelial regeneration began to appear (Figure 3D). In concordance with the histological assessment, treatment with rIL-33 resulted in increased gene expression of pro-inflammatory cytokines (*Il1b*, *Il6*, and *Tnf*) and chemokines (*Ccl2*, *Cxcl1*, *Cxcl2*, *Cxcl9*, and *Cxcl10*) in lung tissue at D4 (Figure 3E). Together, these findings indicate that exogenous IL-33 exacerbates lung inflammation and immunopathogenesis in the context of SARS-CoV-2 infection.

IL-33 modulates pulmonary immune signatures in SARS-CoV-2 infection

To identify the unique immune signature induced by IL-33 during SARS-CoV-2 infection, we prepared lung homogenates from WT and IL-33$^{-/-}$ mice and performed a bulk RNA-seq assay. Principal component analysis revealed distinct transcriptional signatures of WT and IL-33$^{-/-}$ samples at each time point (Figure S3). The gene set enrichment analysis conducted with Molecular Signatures Database (MSigDB) displayed robust antiviral immune responses in the lungs of infected mice on both D2 and D4 compared to uninfected mice (Figures S4A and S4B). The volcano plot shows that expression of 1,374 genes is upregulated and that expression of 967 genes is downregulated in the lungs of IL-33$^{-/-}$ mice when compared to the lungs of WT mice at D2 (Figure 4A). Notably, hallmark pathways associated with immune and inflammatory responses, including IFN-I/IFN-γ, TNF/NF-κB, IL-6/JAK/STAT3, and IL-2/STAT signaling pathways were downregulated in the lungs of IL-33$^{-/-}$ mice on D2 (Figure 4B). In contrast, hallmark pathways related to epithelial-mesenchymal transition, apical junction, and Hedgehog signaling were upregulated in IL-33$^{-/-}$ mice (Figure 4B). As shown in Figure 4C, downregulated genes in the IFN-γ signaling pathway included cytokines (*Ifng*, *Il6*, *Il1b*, and *Ifnb1*), chemokines (*Cxcl9* and *Cxcl10*), interferon stimulated genes (*Ifit2*, *Isg15*, *Irf8*, and *Irf1*), transcription regulators (*Spl1*, *SOCS1*, and *SOCS3*), immunoproteasome (*PSMB9*), oxidase (*Cybb*/*Nox2*), protein kinase C member (*Prkcd*), and peptide transporter (*Tap1*). We further illustrated the gene network of IL-33 and COVID-19 by ingenuity pathway analysis (IPA) analysis (Figure 4D) and found that IL-33 tightly regulated several inflammatory cytokines/chemokines. These included *Ifng*, *Cxcl8*, *Cxcl2*, *Cxcl10*, *Ccl2*, *Tnf*, *Il4*, *Il6*, *Il10*, *Il13*, and *Il1b*, all of which are critical components that contribute to the CS observed in severe COVID-19. The pathway network revealed that IL-33 deficiency resulted in downregulation of lymphocyte/granulocyte activation, dendritic cell maturation, and pathogen-induced CS signaling (Figure 4E). The IFN/STAT signaling pathway and the inflammatory cytokines IL-17A, IL-18, IL-27, and TNF were also downregulated in the absence of IL-33, which suggests that IL-33 is a key endogenous danger signal for lung inflammation. In addition, suppressor of cytokine signaling 3 (SOCS3), an important regulator of inflammation that inhibits STAT activation, was significantly upregulated in IL-33-deficient mice following SARS-CoV-2 infection. Interestingly, IL-33 deficiency resulted in an increase in IL-1 receptor antagonist (IL1RN) levels (Figure 4E). Since IL1RN inhibits the pro-inflammatory effect of IL-1β, it could potentially contribute to the reduction of IL-1β-mediated pulmonary inflammation during infection in IL-33$^{-/-}$ mice.

The analysis of the CS signaling pathway revealed inhibition of MyD88, AP-1, and NF-κB signals in the absence of IL-33, which could lead to the reduced production of IL-6 and TNF-α (Figures S5 and S6). Decreased NF-κB activation in IL-33$^{-/-}$ mice also caused a reduction in interferon regulatory factor 1 (IRF-1), and limited CCL5 and CXCL10 production, resulting in attenuated immune infiltration in the lungs. In addition, IL-33-deficiency may prevent immune cell (e.g., macrophages, NK, Th1, and Th17 cells) activation and migration via downregulation of cytokine/chemokine receptors including IL-12R, IL-21R, TNFR, CCR1, and CCR5, thus alleviating inflammatory cytokine secretion and immunopathogenesis. Furthermore, the absence of IL-33 led to a decrease in the expression of Toll-like receptors (TLR), specifically TLR1, 2, 3, and 7, which play a critical role in recognizing viruses by host cells. Downregulation of TLRs may also dampen NF-κB signaling and limit inflammatory cytokine production (Figure S6). A limited number of differentially expressed genes in the lungs were also identified between knockout and WT mice on D4 (127 gene upregulation and 198 gene downregulation), which was a similar trend to that observed on D2 (Figure S7). Altogether, the RNA-seq analysis demonstrated that IL-33 plays a pivotal role in initiating inflammatory responses via activating several signaling pathways. Therapeutic interventions toward IL-33 signaling hold promise as a potential avenue for addressing severe COVID-19.

DISCUSSION

COVID-19 has caused more than 6.9 million deaths worldwide as of November 2023. Severe COVID-19 not only causes significant damage to lung tissue, but it also affects other organs, such as the heart, kidneys, and brain which can result in long-term sequelae.[26,27] Recent evidence

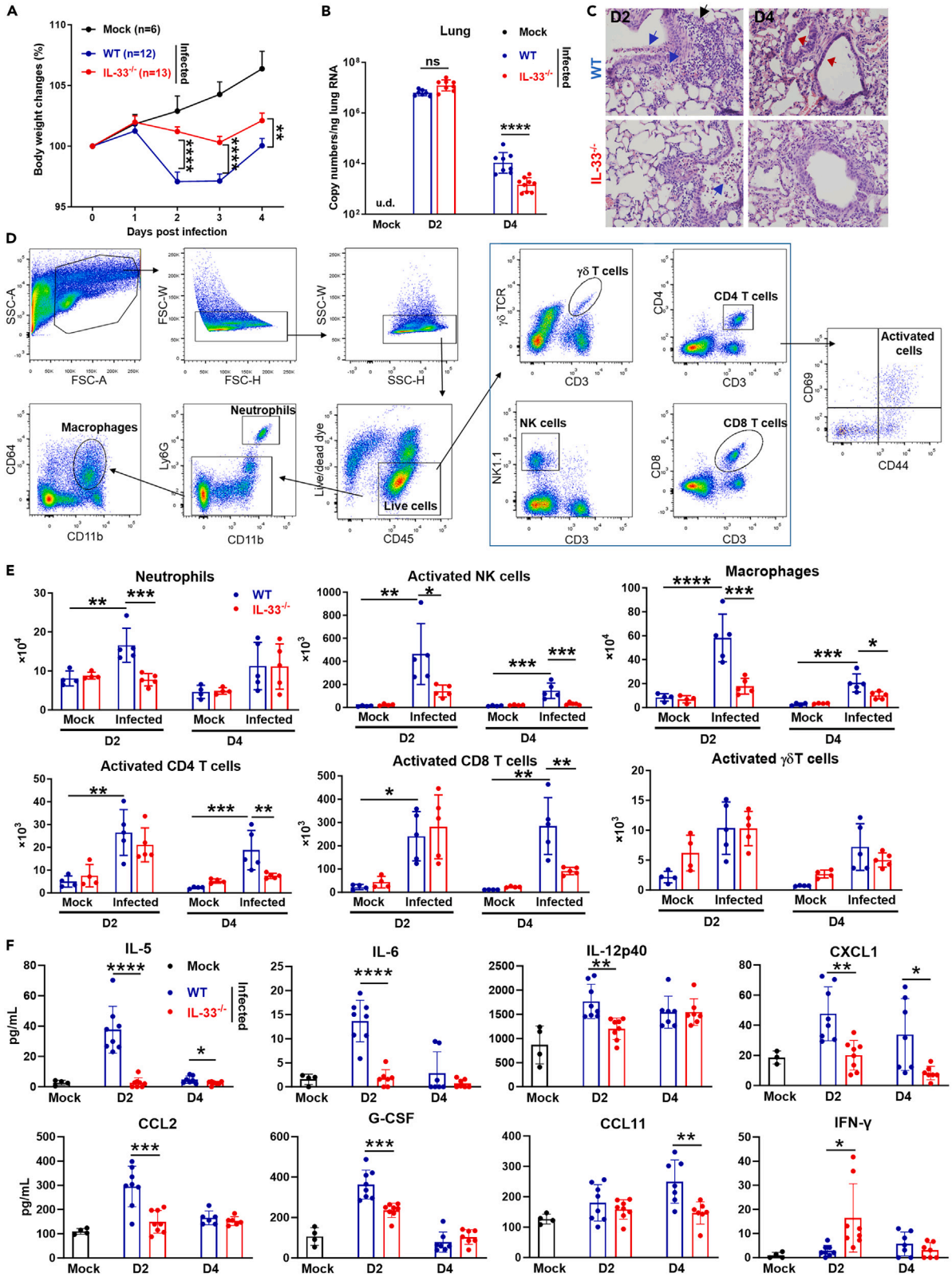
A
Mock (n=6)
WT (n=12)
IL-33-/- (n=13)
Infected
Body weight changes (%)
Days post infection
B
Lung
Mock
WT
IL-33-/-
Infected
Copy numbers/ng lung RNA
ns
u.d.
Mock
D2
D4
C
D2
D4
WT
IL-33-/-
D
SSC-A
FSC-A
FSC-W
FSC-H
SSC-W
SSC-H
Macrophages
CD64
CD11b
Neutrophils
Ly6G
Live/dead dye
Live cells
CD45
γδ T cells
γδ TCR
CD3
CD4 T cells
CD4
NK cells
NK1.1
CD8 T cells
CD8
Activated cells
CD69
CD44
E
Neutrophils
Activated NK cells
Macrophages
Activated CD4 T cells
Activated CD8 T cells
Activated γδT cells
WT
IL-33-/-
Mock
Infected
D2
D4
F
IL-5
IL-6
IL-12p40
CXCL1
CCL2
G-CSF
CCL11
IFN-γ
pg/mL
Mock
WT
IL-33-/-
Infected

Figure 2. IL-33 deficiency alleviated SARS-CoV-2-induced pulmonary inflammation in mice

WT B6 and IL-33$^{-/-}$ mice were infected with SARS-CoV-2 as indicated in Figure 1. B6 mice in the mock group were i.n. treated with the same volume of cell culture medium.

(A) Bodyweight changes of WT and IL-33$^{-/-}$ mice after SARS-CoV-2 infection. Data were pooled from two independent experiments and were analyzed by repeated measures two-way ANOVA.

(B) Relative viral load was measured by RT-qPCR; bar graph represents as a mean ± SD (n = 7–8/group). These data were analyzed by t tests at each time point.

(C) Histological changes in the lungs of WT and IL-33$^{-/-}$ mice after SARS-CoV-2 infection: immune cell infiltration (black arrow), intrabronchial mucus and cell debris (blue arrows) and epithelial regeneration (red arrows).

(D) Gating strategy flow cytometry data. Lymphocytes were selected from a forward scatter-A vs. side scatter-A dot plot, and single cells were subsequently selected. Then, live lymphocytes were selected by live/dead dye and CD45. Neutrophils were identified as Ly6G^{+} cells. Macrophages were identified as CD11b^{+}CD64^{+} cells. T cells were first identified as CD3^{+} and further subdivided into CD4^{+} and CD8^{+} T cells. NK cells were identified as CD3^{-} and NK1.1^{+}. γδT cells were identified as CD3^{+} and γδTCR^{+}. CD44^{+}CD69^{+} population was characterized as activated cells.

(E) Flow cytometric analysis of lung tissues of WT and IL-33$^{-/-}$ mice at days 2 and 4 post-SARS-CoV-2 infection. The numbers of neutrophils, activated NK cells, macrophages, activated CD4 T cells, activated CD8 T cells and activated γδ T cells were plotted. Bar graph represents as a mean ± SD (n = 4–5/group) (one-way ANOVA followed by Tukey's multiple comparison test at each time point).

(F) Protein levels of IL-5, IL-6, IL-12p40, IFN-g, G-CSF, CXCL1, CCL2, and CCL-11 in the serum of WT and IL-33$^{-/-}$ mice after SARS-CoV-2 infection. Data were analyzed by unpaired/two-tailed t tests at each time point. All results are presented as the mean ± SD, and this experiment was performed twice independently with similar trends. Statistically significant values are denoted as *p < 0.05, **p < 0.01, ***p < 0.001, and ****p < 0.0001.

suggests that dysregulation of the host immune system could be responsible for COVID-19 pathogenesis, including lymphopenia, neutrophilia, dysregulated monocyte and macrophage activation, inhibited or delayed IFN-I response, and CS. Therefore, identifying key factors that mediate immune dysregulation is warranted and can be translationally relevant. In the present study, our results demonstrated a positive correlation between IL-33 levels and COVID-19 severity in patient samples. These findings corroborate recent reports from other groups.[20,21,28] Of note, we reported that IL-33 is present in naso-/oro-pharyngeal swab samples and positively correlates with severe COVID-19 and thus might represent a potential target for predicting disease severity as used in acute asthma.[29] Here, we demonstrated that IL-33 was significantly upregulated in the lungs in two murine models (Figures 1 and S1) and was accompanied by extensive inflammatory gene expression, including IFN-I, IFN-γ, IL-6, and TNF. Strong upregulation of CXCL1/2 and CCL2 may also contribute to robust neutrophil and macrophage infiltration in the lung tissue. In contrast, the alteration of type II cytokines (IL-4, IL-13, and IL-10) was relatively mild (Figure 1). Increased levels of serum IL-5 have been reported in critically ill COVID-19 patients,[30] and we also observed a strong increase in serum IL-5 at day 2 in mice. Next, we explored the role of IL-33 in animal models using two strategies that included an IL-33 knockout (endogenous) and treatment with recombinant IL-33 (exogenous) (Figures 2 and 3). Although IL-33 may not play a major role in controlling SARS-CoV-2 early in the course of infection, proinflammatory cytokines and chemokines were closely regulated by IL-33 in both lung tissue and blood. Intriguingly, IL-33$^{-/-}$ mice showed an increased trend of IFN-γ levels in the blood, suggesting that endogenous IL-33 signal deficiency may induce systemic IFN-γ during the acute stage of inflammation as reported by others in ConA-induced hepatitis.[31]

Our histological assessment indicated that IL-33 contributes to pathological changes in the lungs. This is highly likely due to elevated immune cell infiltration and activation in the lungs. We confirmed this hypothesis using flow cytometry. Flow cytometric analysis showed that the absence of IL-33 resulted in lower myeloid cell infiltrates in the lungs. The number of activated T cells was also lower in IL-33$^{-/-}$ mice at day 4, suggesting that IL-33 may also promote adaptive immune cell activation in SARS-CoV-2 infection. IL-33 can regulate γδ T cell activation and differentiation in lymphocytic choriomeningitis virus (LCMV) infection;[16] however, we did not observe any changes of activated γδ T cell numbers in our SARS-CoV-2 mouse model (Figure 2).

Our RNA-seq assay provided evidence to suggest that IL-33 plays a key role in the induction of hyperinflammation. As shown in Figure S4, SARS-CoV-2 infection induced activation of hyperinflammatory pathways in the lungs, including TNF/NF-κB, IFN-I/II, IL-6/JAK/STAT2, IL-2/STAT5, and complement. These signal pathways were all downregulated in IL-33$^{-/-}$ mice (Figure 4), indicating that IL-33 may act as an amplifier of inflammation via recruitment and activation of inflammatory cells such as macrophages, neutrophils, NK cells, and T cells. The IPA network also generated a link between IL-33 and various proinflammatory cytokines that are known to mediate lung damage in severe COVID-19 (Figure 4D). Moreover, IL-33 is reported to trigger a MyD88-and NF-κB-dependent acute inflammatory response.[32] The fact that IL-33 signaling is critical for NF-κB-dependent inflammation in the lungs (Figure S5) suggests that targeting of IL-33/NF-κB axis could be a promising therapeutic target to attenuate lung pathology in severe COVID-19. Of note, IL-33 may also promote Th2 differentiation and ILC2 activation via NF-κB activation, which leads to pulmonary fibrosis.[33–38] More research is needed to illustrate the exact role(s) of IL-33 during the recovery stages of COVID-19.

Limitations of the study

Although we revealed a critical role of IL-33 in SARS-CoV-2 infection, our mouse model is a limitation of this study. Given that our mouse model is a rapidly self-recovering model, we were unable to investigate the role of IL-33 in long-term SARS-CoV-2 infection. Further studies are needed to explore the specific role(s) of IL-33 in long COVID and might utilize K18hACE2 or humanized mice. Although our model is a non-lethal model, various types of transgenic mice, most of which are on B6 background, can be leveraged in the future to identify other key molecules that are involved in immune dysregulation *in vivo*. Altogether, our study demonstrates a vital role of IL-33 in lung hyperinflammation and pathology in SARS-CoV-2-infected mice and highlights IL-33 as a potential therapeutic target for severe COVID-19.

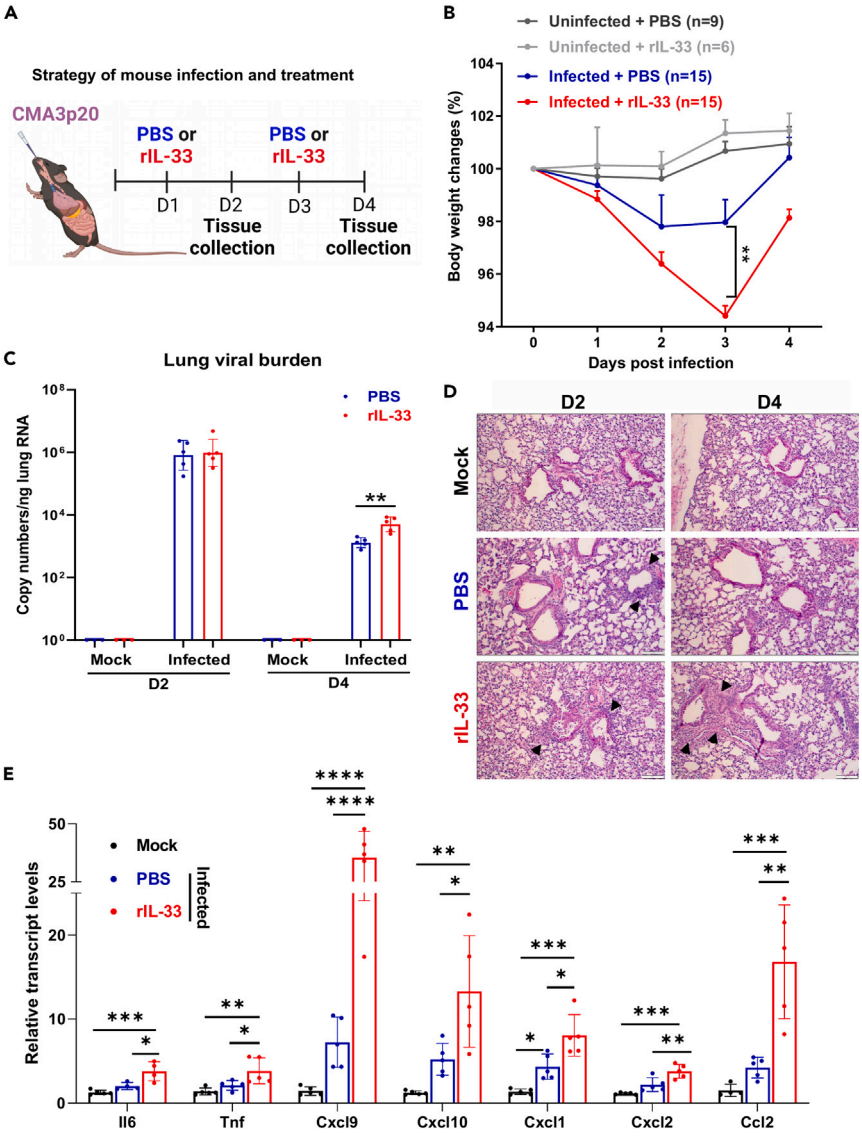

Figure 3. Exogenous IL-33 exacerbated SARS-CoV-2-induced lung inflammation and pathology

(A) Schematic of SARS-CoV-2 infection (Created with BioRender.com). B6 mice were i.n. infected with 5 × 10^5 PFU CMA3p20, followed by intraperitoneal administration of PBS or recombinant IL-33 (rIL-33). Uninfected mice with or without rIL-33 treatment were used as controls. Lung tissues were harvested at D2 and D4. The illustration was created with BioRender.com.

(B) Bodyweight changes in mice post SARS-CoV-2 infection and treatment. Data were pooled from two independent experiments and were analyzed by repeated measures two-way ANOVA.

(C) Lung viral loads were measured by RT-qPCR and these data were analyzed by unpaired/two-tailed t tests at each time point.

(D) Representative H&E staining images of lungs. Scale bars, 100 μm. Immune cell infiltration into alveolar spaces (lung consolidation), chronic fibrosis and bronchial epithelial regeneration (arrows) were observed in lung sections from SARS-CoV-2 infected mice.

(E) Relative transcript levels of the indicated genes in the lungs at D4 were analyzed by RT-qPCR (n = 4–5/group). These data were analyzed by one-way ANOVA, followed by Tukey's multiple comparison test. All results are presented as the mean ± SD, and this experiment was performed twice independently with similar trends. Statistically significant values are denoted as *p < 0.05, **p < 0.01, ***p < 0.001, and ****p < 0.0001.

STAR★METHODS

Detailed methods are provided in the online version of this paper and include the following:

- KEY RESOURCES TABLE
- RESOURCE AVAILABILITY

A

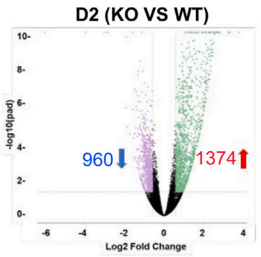

B

Top ten Hallmark at D2 (KO vs WT)	GSEA p-Adj	GSEA score	p-Adj	Up gene #	Down gene #
HALLMARK_INTERFERON_GAMMA_RESPONSE	0.00083	-0.7360	0	3	79
HALLMARK_EPITHELIAL_MESENCHYMAL_TRANSITION	0.00068	0.5529	0	52	13
HALLMARK_TNFA_SIGNALING_VIA_NFKB	0.00083	-0.6945	1.2e-09	4	60
HALLMARK_INTERFERON_ALPHA_RESPONSE	0.00083	-0.7812	3.9e-08	1	36
HALLMARK_APICAL_JUNCTION	0.00347	0.4848	0.00116	33	15
HALLMARK_IL6_JAK_STAT3_SIGNALING	0.00083	-0.6069	0.00169	4	21
HALLMARK_HEDGEHOG_SIGNALING	0.00395	0.7046	0.00198	13	1
HALLMARK_INFLAMMATORY_RESPONSE	0.00083	-0.5842	0.00220	6	40
HALLMARK_IL2_STAT5_SIGNALING	0.00343	-0.4196	0.00320	13	33
HALLMARK_ALLOGRAFT_REJECTION	0.00083	-0.6181	0.00489	3	41

C

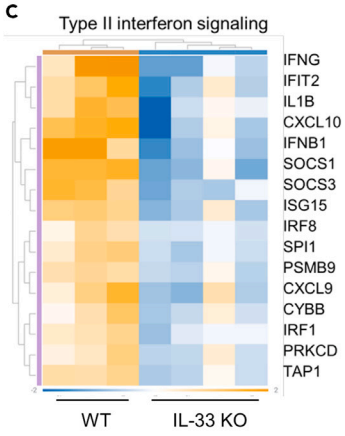

D

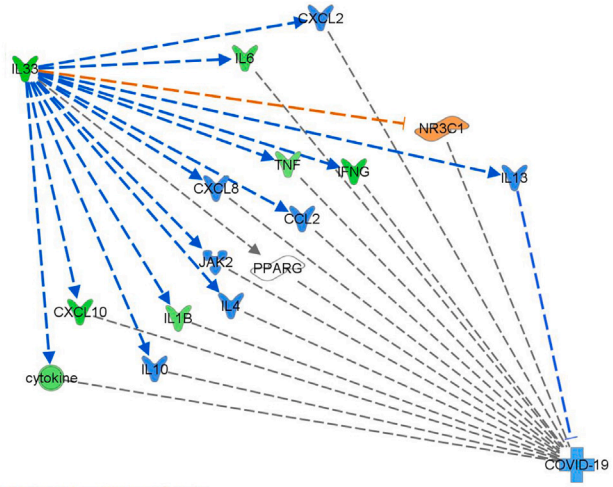

E

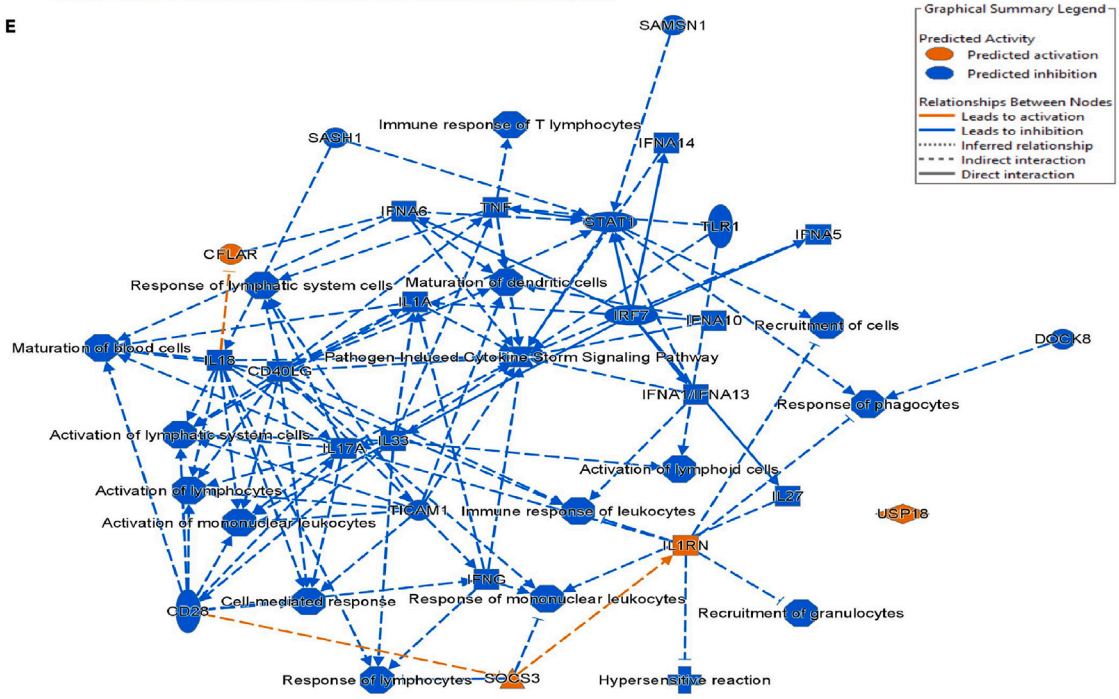

Figure 4. IL-33 regulated inflammatory signaling pathways in SARS-CoV-2-infection

WT B6 and IL-33$^{-/-}$ mice were infected with SARS-CoV-2 as indicated in Figure 1 (n = 3–5 mice/group). B6 mice in the mock group were i.n. treated with the same volume of cell culture medium. Lungs were perfused with cold PBS and harvested for RNA extraction and RNA-seq analysis.

(A) Volcano plot describing the fold changes and false discovery rate (FDR)-adjusted p values between infected WT and IL-33$^{-/-}$ lungs on D2.

(B) Pathway enrichment analysis of top ten hallmark pathways in the lungs on D2.

Figure 4. *Continued*

(C) Representative heatmaps of differently expressed genes of IFN-γ signaling pathway in the lungs of WT and IL-33$^{-/-}$ mice on D2. Heatmaps were generated based on KEGG pathway using the Rosalind platform.

(D) Network plot showing the genes correlating IL-33 to the COVID-19 disease database identified by ingenuity pathway analysis of the bulk RNA-seq. The orange and green labels indicate upregulation and downregulation, respectively, when compare IL-33$^{-/-}$ to WT samples.

(E) The network of differently expressed genes, pathways and cell functions analyzed by IPA network analyzer. The orange and blue legend on the right indicates the genes predicted to be activation or inhibition, respectively.

SUPPLEMENTAL INFORMATION

Supplemental information can be found online at https://doi.org/10.1016/j.isci.2024.110117.

ACKNOWLEDGMENTS

We would like to thank the UTMB Flow Cytometry and Cell Sorting Core (Meredith Weglarz) for flow cytometry assistance and Ashley Smith for manuscript revision. This work was supported partially by the National Institute of Allergy and Infectious Diseases grants (AI153586 to Y.L. and AI132674 to L.S.), a UTMB IHII NTT Startup grant (to Y.L.), a COVID-19 and Emerging Respiratory Viruses Research Award from American Lung Association (COVID-920427 to Y.M.H.), COVID-19 Bridging grant from Sealy Institute for Vaccine Sciences (C28455 to Y.M.H.), UTMB IHII COVID-19 Pilot grant supported by Sealy & Smith Foundation (85393 to Y.M.H.). H.W. is supported by IHII Data Acquisition grant and Gulf Coast Center for Precision Environmental Health Pilot Project. P.S. and X.X. were supported by Sealy & Smith Foundation, Kleberg Foundation, John S. Dunn Foundation, Amon G. Carter Foundation, Gilson Longenbaugh Foundation, and Summerfield Robert Foundation. The funders had no roles in study design, data collection and analysis, decision to publish, or preparation of the manuscript. This research was conducted using samples provided by the Biorepository for Severe Emerging Infections at the University of Texas Medical Branch. The authors are grateful to the participants who made this study possible by donating samples.

AUTHOR CONTRIBUTIONS

Conceptualization, H.W. and Y.L.; data curation, H.W., C.G., and Y.L.; formal analysis, H.W., Y.Z., X.Y., and Y.L.; funding acquisition, H.W., L.S., and Y.L.; investigation, H.W., Y.M.H., P.J.B., and Y.L.; methodology, H.W., Y.M.H., and Y.L.; resources, C.B.L., S.M., N.C., X.X., P.-Y.S., P.R., and L.S.; supervision, Y.L.; validation, Y.L.; visualization, H.W., P.J.B., C.G., and Y.L.; writing, H.W. and Y.L.; writing – review and editing, H.W., Y.M.H., P.J.B., J.Y., Y.Z., X.Y., X.X., H.H., K.S., L.S., J.S., and Y.L.

DECLARATION OF INTERESTS

The authors declare no competing interests.

DECLARATION OF GENERATIVE AI AND AI-ASSISTED TECHNOLOGIES IN THE WRITING PROCESS

During the preparation of this work the author YL used ChatGPT in order to improve readability and language. After using this tool, the author reviewed and edited the content as needed and takes full responsibility for the content of the publication.

Received: December 13, 2023
Revised: March 5, 2024
Accepted: May 23, 2024
Published: May 27, 2024

REFERENCES

1. Huang, C., Wang, Y., Li, X., Ren, L., Zhao, J., Hu, Y., Zhang, L., Fan, G., Xu, J., Gu, X., et al. (2020). Clinical features of patients infected with 2019 novel coronavirus in Wuhan, China. Lancet *395*, 497–506.
2. Blanco-Melo, D., Nilsson-Payant, B.E., Liu, W.C., Uhl, S., Hoagland, D., Møller, R., Jordan, T.X., Oishi, K., Panis, M., Sachs, D., et al. (2020). Imbalanced Host Response to SARS-CoV-2 Drives Development of COVID-19. Cell *181*, 1036–1045.e9. https://doi.org/10.1016/j.cell.2020.04.026.
3. Fajgenbaum, D.C., and June, C.H. (2020). Cytokine Storm. N. Engl. J. Med. *383*, 2255–2273.
4. Montazersaheb, S., Hosseiniyan Khatibi, S.M., Hejazi, M.S., Tarhriz, V., Farjami, A., Ghasemian Sorbeni, F., Farahzadi, R., and Ghasemnejad, T. (2022). COVID-19 infection: an overview on cytokine storm and related interventions. Virol. J. *19*, 92. https://doi.org/10.1186/s12985-022-01814-1.
5. McLean, G., Kamil, J., Lee, B., Moore, P., Schulz, T.F., Muik, A., Sahin, U., Türeci, Ö., and Pather, S. (2022). The Impact of Evolving SARS-CoV-2 Mutations and Variants on COVID-19 Vaccines. mBio *13*, e0297921. https://doi.org/10.1128/mbio.02979-21.
6. Yang, L., Xie, X., Tu, Z., Fu, J., Xu, D., and Zhou, Y. (2021). The signal pathways and treatment of cytokine storm in COVID-19. Signal Transduct. Targeted Ther. *6*, 255. https://doi.org/10.1038/s41392-021-00679-0.
7. Declercq, J., Van Damme, K.F.A., De Leeuw, E., Maes, B., Bosteels, C., Tavernier, S.J., De Buyser, S., Colman, R., Hites, M., Verschelden, G., et al. (2021). Effect of anti-interleukin drugs in patients with COVID-19 and signs of cytokine release syndrome (COV-AID): a factorial, randomised, controlled trial. Lancet Respir. Med. *9*, 1427–1438. https://doi.org/10.1016/S2213-2600(21)00377-5.
8. Stone, J.H., Frigault, M.J., Serling-Boyd, N.J., Fernandes, A.D., Harvey, L., Foulkes, A.S., Horick, N.K., Healy, B.C., Shah, R., Bensaci, A.M., et al. (2020). Efficacy of Tocilizumab in Patients Hospitalized with Covid-19. N. Engl. J. Med. *383*, 2333–2344. https://doi.org/10.1056/NEJMoa2028836.
9. Soin, A.S., Kumar, K., Choudhary, N.S., Sharma, P., Mehta, Y., Kataria, S., Govil, D., Deswal, V., Chaudhry, D., Singh, P.K., et al. (2021). Tocilizumab plus standard care versus standard care in patients in India with moderate to severe COVID-19-associated cytokine release syndrome (COVINTOC): an open-label, multicentre, randomised, controlled, phase 3 trial. Lancet Respir. Med. *9*, 511–521. https://doi.org/10.1016/S2213-2600(21)00081-3.
10. Patel, J., Bass, D., Beishuizen, A., Bocca Ruiz, X., Boughanmi, H., Cahn, A., Colombo, H., Criner, G.J., Davy, K., de-Miguel-Díez, J., et al. (2023). A randomised trial of anti-GM-CSF otilimab in severe COVID-19 pneumonia (OSCAR). Eur. Respir. J. *61*, 2101870. https://doi.org/10.1183/13993003.01870-2021.
11. Gong, T., Liu, L., Jiang, W., and Zhou, R. (2020). DAMP-sensing receptors in sterile inflammation and inflammatory diseases. Nat. Rev. Immunol. *20*, 95–112. https://doi.org/10.1038/s41577-019-0215-7.
12. Drake, L.Y., and Kita, H. (2017). IL-33: biological properties, functions, and roles in airway disease. Immunol. Rev. *278*, 173–184. https://doi.org/10.1111/imr.12552.
13. Liang, Y., Yi, P., Yuan, D.M.K., Jie, Z., Kwota, Z., Soong, L., Cong, Y., and Sun, J. (2019). IL-33 induces immunosuppressive neutrophils via a type 2 innate lymphoid cell/IL-13/STAT6 axis and protects the liver against injury in LCMV infection-induced viral hepatitis. Cell. Mol. Immunol. *16*, 126–137.
14. Liang, Y., Jie, Z., Hou, L., Aguilar-Valenzuela, R., Vu, D., Soong, L., and Sun, J. (2013). IL-33 induces nuocytes and modulates liver injury in viral hepatitis. J. Immunol. *190*, 5666–5675.
15. Liang, Y., Ge, Y., and Sun, J. (2021). IL-33 in COVID-19: friend or foe? Cell. Mol. Immunol. *18*, 1602–1604.
16. Liang, Y., Jie, Z., Hou, L., Yi, P., Wang, W., Kwota, Z., Salvato, M., de Waal Malefyt, R., Soong, L., and Sun, J. (2015). IL-33 promotes innate IFN-gamma production and modulates dendritic cell response in LCMV-induced hepatitis in mice. Eur. J. Immunol. *45*, 3052–3063. https://doi.org/10.1002/eji.201545696.
17. Cayrol, C., and Girard, J.P. (2018). Interleukin-33 (IL-33): A nuclear cytokine from the IL-1 family. Immunol. Rev. *281*, 154–168.
18. Dwyer, G.K., D'Cruz, L.M., and Turnquist, H.R. (2022). Emerging Functions of IL-33 in Homeostasis and Immunity. Annu. Rev. Immunol. *40*, 15–43. https://doi.org/10.1146/annurev-immunol-101320-124243.
19. Bonilla, W.V., Fröhlich, A., Senn, K., Kallert, S., Fernandez, M., Johnson, S., Kreutzfeldt, M., Hegazy, A.N., Schrick, C., Fallon, P.G., et al. (2012). The alarmin interleukin-33 drives protective antiviral CD8$^+$ T cell responses. Science *335*, 984–989. https://doi.org/10.1126/science.1215418.
20. Stanczak, M.A., Sanin, D.E., Apostolova, P., Nerz, G., Lampaki, D., Hofmann, M., Steinmann, D., Krohn-Grimberghe, M., Thimme, R., Mittler, G., et al. (2021). IL-33 expression in response to SARS-CoV-2 correlates with seropositivity in COVID-19 convalescent individuals. Nat. Commun. *12*, 2133.
21. Markovic, S.S., Jovanovic, M., Gajovic, N., Jurisevic, M., Arsenijevic, N., Jovanovic, M., Jovanovic, M., Mijailovic, Z., Lukic, S., Zornic, N., et al. (2021). IL 33 Correlates With COVID-19 Severity, Radiographic and Clinical Finding. Front. Med. *8*, 749569.
22. Majeed, A.Y., Zulkafli, N.E.S., and Ad'hiah, A.H. (2023). Interleukin-22 and interleukin-33 show up-regulated levels in the serum of patients with mild/moderate Coronavirus disease 2019. Beni. Suef. Univ. J. Basic Appl. Sci. *12*, 24. https://doi.org/10.1186/s43088-023-00367-8.
23. Furci, F., Murdaca, G., Allegra, A., Gammeri, L., Senna, G., and Gangemi, S. (2022). IL-33 and the Cytokine Storm in COVID-19: From a Potential Immunological Relationship towards Precision Medicine. Int. J. Mol. Sci. *23*, 14532. https://doi.org/10.3390/ijms232314532.
24. Gao, Y., Cai, L., Li, L., Zhang, Y., Li, J., Luo, C., Wang, Y., and Tao, L. (2022). Emerging Effects of IL-33 on COVID-19. Int. J. Mol. Sci. *23*, 13656. https://doi.org/10.3390/ijms232113656.
25. Muruato, A., Vu, M.N., Johnson, B.A., Davis-Gardner, M.E., Vanderheiden, A., Lokugamage, K., Schindewolf, C., Crocquet-Valdes, P.A., Langsjoen, R.M., Plante, J.A., et al. (2021). Mouse-adapted SARS-CoV-2 protects animals from lethal SARS-CoV challenge. PLoS Biol. *19*, e3001284. https://doi.org/10.1371/journal.pbio.3001284.
26. Stein, S.R., Ramelli, S.C., Grazioli, A., Chung, J.Y., Singh, M., Yinda, C.K., Winkler, C.W., Sun, J., Dickey, J.M., Ylaya, K., et al. (2022). SARS-CoV-2 infection and persistence in the human body and brain at autopsy. Nature *612*, 758–763. https://doi.org/10.1038/s41586-022-05542-y.
27. Puelles, V.G., Lütgehetmann, M., Lindenmeyer, M.T., Sperhake, J.P., Wong, M.N., Allweiss, L., Chilla, S., Heinemann, A., Wanner, N., Liu, S., et al. (2020). Multiorgan and Renal Tropism of SARS-CoV-2. N. Engl. J. Med. *383*, 590–592. https://doi.org/10.1056/NEJMc2011400.
28. Zeng, Z., Hong, X.Y., Li, Y., Chen, W., Ye, G., Li, Y., and Luo, Y. (2020). Serum-soluble ST2 as a novel biomarker reflecting inflammatory status and illness severity in patients with COVID-19. Biomarkers Med. *14*, 1619–1629.
29. Poulsen, N.N., Bjerregaard, A., Khoo, S.K., Laing, I.A., Le Souëf, P., Backer, V., Rapley, L., Cohen, S.E., Barrett, L., Thompson, P., et al. (2018). Airway Interleukin-33 and type 2 cytokines in adult patients with acute asthma. Respir. Med. *140*, 50–56. https://doi.org/10.1016/j.rmed.2018.05.016.
30. Ju, X., Son, K., Jamil, R., Culgin, S., Salter, B., Miyasaki, K., Fard, N.E., Xiao, M., Patel, Z., Zhang, K., et al. (2023). Eosinophil-independent IL-5 levels are increased in critically ill COVID-19 patients who survive. Allergy Asthma Clin. Immunol. *19*, 58. https://doi.org/10.1186/s13223-023-00810-6.
31. Volarevic, V., Mitrovic, M., Milovanovic, M., Zelen, I., Nikolic, I., Mitrovic, S., Pejnovic, N., Arsenijevic, N., and Lukic, M.L. (2012). Protective role of IL-33/ST2 axis in Con A-induced hepatitis. J. Hepatol. *56*, 26–33. https://doi.org/10.1016/j.jhep.2011.03.022.
32. Liew, F.Y., Girard, J.P., and Turnquist, H.R. (2016). Interleukin-33 in health and disease. Nat. Rev. Immunol. *16*, 676–689.
33. Schmitz, J., Owyang, A., Oldham, E., Song, Y., Murphy, E., McClanahan, T.K., Zurawski, G., Moshrefi, M., Qin, J., Li, X., et al. (2005). IL-33, an interleukin-1-like cytokine that signals via the IL-1 receptor-related protein ST2 and induces T helper type 2-associated cytokines. Immunity *23*, 479–490.
34. Zaini, A., Fulford, T.S., Grumont, R.J., Runting, J., Rodrigues, G., Ng, J., Gerondakis, S., Zaph, C., and Scheer, S. (2021). c-Rel Is Required for IL-33-Dependent Activation of ILC2s. Front. Immunol. *12*, 667922. https://doi.org/10.3389/fimmu.2021.667922.
35. Zhang, J., Qiu, J., Zhou, W., Cao, J., Hu, X., Mi, W., Su, B., He, B., Qiu, J., and Shen, L. (2022). Neuropilin-1 mediates lung tissue-specific control of ILC2 function in type 2 immunity. Nat. Immunol. *23*, 237–250. https://doi.org/10.1038/s41590-021-01097-8.
36. Li, D., Guabiraba, R., Besnard, A.G., Komai-Koma, M., Jabir, M.S., Zhang, L., Graham, G.J., Kurowska-Stolarska, M., Liew, F.Y., McSharry, C., and Xu, D. (2014). IL-33 promotes ST2-dependent lung fibrosis by the induction of alternatively activated macrophages and innate lymphoid cells in mice. J. Allergy Clin. Immunol. *134*, 1422–1432.e11. https://doi.org/10.1016/j.jaci.2014.05.011.
37. Hams, E., Armstrong, M.E., Barlow, J.L., Saunders, S.P., Schwartz, C., Cooke, G., Fahy, R.J., Crotty, T.B., Hirani, N., Flynn, R.J., et al. (2014). IL-25 and type 2 innate lymphoid cells induce pulmonary fibrosis. Proc. Natl. Acad. Sci. USA *111*, 367–372.

38. Fonseca, W., Lukacs, N.W., Elesela, S., and Malinczak, C.A. (2021). Role of ILC2 in Viral-Induced Lung Pathogenesis. Front. Immunol. *12*, 675169.
39. Liu, Y., Liu, J., Johnson, B.A., Xia, H., Ku, Z., Schindewolf, C., Widen, S.G., An, Z., Weaver, S.C., Menachery, V.D., et al. (2022). Delta spike P681R mutation enhances SARS-CoV-2 fitness over Alpha variant. Cell Rep. *39*, 110829. https://doi.org/10.1016/j.celrep.2022.110829.
40. Liang, Y., Wang, X., Wang, H., Yang, W., Yi, P., Soong, L., Cong, Y., Cai, J., Fan, X., and Sun, J. (2022). IL-33 activates mTORC1 and modulates glycolytic metabolism in CD8(+) T cells. Immunology *165*, 61–73.
41. Harcourt, J., Tamin, A., Lu, X., Kamili, S., Sakthivel, S.K., Murray, J., Queen, K., Tao, Y., Paden, C.R., Zhang, J., et al. (2020). Severe Acute Respiratory Syndrome Coronavirus 2 from Patient with Coronavirus Disease, United States. Emerg. Infect. Dis. *26*, 1266–1273. https://doi.org/10.3201/eid2606.200516.
42. Wang, L., Wang, S., and Li, W. (2012). RSeQC: quality control of RNA-seq experiments. Bioinformatics *28*, 2184–2185. https://doi.org/10.1093/bioinformatics/bts356.
43. Anders, S., Pyl, P.T., and Huber, W. (2015). HTSeq–a Python framework to work with high-throughput sequencing data. Bioinformatics *31*, 166–169. https://doi.org/10.1093/bioinformatics/btu638.
44. Love, M.I., Huber, W., and Anders, S. (2014). Moderated estimation of fold change and dispersion for RNA-seq data with DESeq2. Genome Biol. *15*, 550. https://doi.org/10.1186/s13059-014-0550-8.

STAR★METHODS

KEY RESOURCES TABLE

REAGENT or RESOURCE	SOURCE	IDENTIFIER
Antibodies		
Fixable Viability Dye eFluor 506	ThermoFisher Scientific	Cat# 65-0866-14
PE-Cy7-anti-CD3ϵ (145-2C11)	Biolegend	Cat# 100319; RRID: AB_312684
Pacific Blue-anti-CD4 (GK1.5)	Biolegend	Cat# 100428; RRID: AB_493647
APC-efluor780-anti-CD8a (53-6.7)	ThermoFisher Scientific	Cat# 47-0081-82; RRID: AB_1272185
APC-anti-Ly6G (1A8-Ly6G)	Biolegend	Cat# 127614; RRID: AB_2227348
PE-CF594-anti-NK1.1 (PK136)	BD Bioscience	Cat# 562864; RRID: AB_2737850
FITC-anti-CD64 (X54-5/7.1)	Biolegend	Cat# 139316; RRID: AB_2566556
Alexa fluor700-anti-CD11b (M1/70)	Biolegend	Cat# 101222; RRID: AB_493705
BV711-anti-CD44 (IM7)	Biolegend	Cat# 103057; RRID: AB_2564214
APC-anti-γδ TCR (GL3)	ThermoFisher Scientific	Cat# 17-5711-82; RRID: AB_842756
FITC-anti-CD69 (H1.2F3)	ThermoFisher Scientific	Cat# 11-0691-82; RRID: AB_465119
PE-anti-CD45 (30-F11)	Biolegend	Cat# 103106; RRID: AB_312971
Recombinant Anti-IL-33 [EPR17831]	Abcam	Cat# ab187060
β-Actin	Cell Signaling Technology	Cat# 4967
Bacterial and virus strains		
Mouse-adapted strain of SARS-CoV-2 (CMA3p20)	Muruato et al.[25]	N/A
Delta SARS-CoV-2	Liu et al.[39]	N/A
Biological samples		
COVID patient plasma samples	UTMB biorepository	N/A
Healthy donor plasma samples	UTMB biorepository	N/A
COVID patient naso-/oro-pharyngeal swab samples	UTMB biorepository	N/A
Chemicals, peptides, and recombinant proteins		
Recombinant IL-33 cytokine	Biolegend	Cat# 580508
RNAprotect Tissue Reagent	Qiagen	Cat# 76106
Trizol	Thermo Fishier Scientific	Cat# 15596026
RNeasy Mini kit	Qiagen	Cat# 74104
iTaq Universal Probes One-Step kit	Bio-Rad	Cat# 1725141
SARS-CoV-2 qPCR Primer & Probe kit	Integrated DNA Technologies	Cat# 10006713
iScript cDNA Synthesis kit	Bio-Rad	Cat# 1708891
iTaq SYBR Green Supermix	Bio-Rad	Cat# 1725124
Red Cell Lysis Buffer	Sigma-Aldrich	Cat# R7757-100ML
Collagenase type IV	Thermo Fishier Scientific	Cat# 17104019
RPMI-1640 Medium	Thermo Fisher Scientific	Cat# 11875093
Fetal bovine serum	Thermo Fisher Scientific	Cat# 16000044
DPBS, pH7.4	Thermo Fisher Scientific	Cat# 10010023
ECL Western Blotting Substrate	Thermo Fisher Scientific	Cat# 32209
RIPA buffer	Cell Signaling Technology	Cat# 9806
Protease inhibitor cocktail	Sigma-Aldrich	Cat# 11836170001
BCA Protein Assay Kit	Thermo Fisher Scientific	Cat# 23225

(*Continued on next page*)

Continued

REAGENT or RESOURCE	SOURCE	IDENTIFIER
Critical commercial assays		
Human IL-33 Quantikine ELISA Kit	R&D	Cat# D3300B
Bio-Plex Pro Mouse Cytokine 23-plex Assay Kit	Bio-Rad	Cat# M60009RDPD
Deposited data		
Mouse lung bulk RNAseq data	This paper	GEO: GSE247370
Experimental raw data in this paper	Mendeley Data	https://data.mendeley.com/datasets/29zmznx7pv/1
Experimental models: Cell lines		
Vero E6 cell	ATCC	Cat# CRL-1586
Experimental models: Organisms/strains		
C57BL/6j mice	Jackson Labs	Cat# 000664
K18-hACE2	Jackson Labs	Cat# 034860
IL-33$^{-/-}$ mice (B6 background)	UTMB	N/A
Oligonucleotides		
Primers for mouse genes, see Table S1	This paper	N/A
Software and algorithms		
Bio-Rad CFX Maestro 1.1	Bio-Rad	https://www.bio-rad.com
FlowJo version 10	BD Bioscience	https://www.flowjo.com/
Bio-Plex Manager 5.0	Bio-Rad	https://www.bio-rad.com
ROSALIND	ROSALIND	https://rosalind.onramp.bio/
Ingenuity Pathway Analysis	Qiagen	https://digitalinsights.qiagen.com/product-login/
GraphPad Prism 10	Dotmatics	https://www.graphpad.com/

RESOURCE AVAILABILITY

Lead contact

Further information and requests for resources should be directed to and will be fulfilled by the lead contact, Yuejin Liang (yu2liang@utmb.edu).

Materials availability

This study did not generate new unique reagents.

Data and code availability

- RNA-seq data have been deposited at GEO and are publicly available as of the date of publication. Accession numbers are listed in the key resources table. All raw data have been deposited at Mendeley and are publicly available as of the date of publication. All other data reported in this paper will be shared by the lead contact upon request.
- This paper does not report original code.
- Any additional information required to reanalyze the data reported in this paper is available from the lead contact upon request.

EXPERIMENTAL MODEL AND STUDY PARTICIPANT DETAILS

For *in vivo* animal studies, male wild-type C57BL/6j mice (WT B6, stock #000664) and K18-hACE2 (stock #034860) were purchased from Jackson Labs (Bar Harbor, ME). IL-33$^{-/-}$ mice (B6 background) were maintained in our animal facility.[13,16,40] Mice were maintained under specific pathogen-free conditions and used at 8-10 weeks of age, following protocols approved by the Institutional Animal Care and Use Committee at the University of Texas Medical Branch (UTMB) in Galveston, TX. All procedures were approved by the Institutional Biosafety Committee, in accordance with Guidelines for Biosafety in Microbiological and Biomedical Laboratories. UTMB operates in compliance with the USDA Animal Welfare Act (Public Law 89-544), the Health Research Extension Act of 1985 (Public Law 99-158), the Public Health Service Policy on Humane Care and Use of Laboratory Animals, and the NAS Guide for the Care and Use of Laboratory Animals (ISBN-13). UTMB is a registered Research Facility under the Animal Welfare Act and has a current assurance on file with the Office of Laboratory Animal Welfare, in compliance with the NIH Policy. The experimental protocols were carried out following ARRIVE guidelines 2.0 for animal experiments.

For studies involving human participants, plasma and nasopharyngeal swab samples were collected from 61 patients diagnosed with COVID-19. Twenty healthy control samples were obtained from the general population. These patients consented to participate in either the Clinical Characterization Protocol for Severe Emerging Infections (UNMC IRB # 146-20-FB/UTMB IRB # 20-0066) or the Observational Protocol for Diseases and Exposures of Public Health Importance (UNMC IRB # 060-20-EP/UTMB IRB # 20-0031). Patient demographics and detailed methods are included in Table S2.

The mouse-adapted strain of SARS-CoV-2 CMA3p20 is based on the sequence of USA-WA1/2020 isolate and was provided by the World Reference Center for Emerging Viruses and Arboviruses (WRCEVA). It was originally obtained from the United States of America Centers for Disease Control and Prevention.[25,41] Delta SARS-CoV-2 was also used as reported in our previous publication.[39] Viruses were titrated and propagated in Vero E6 cells and then grown in DMEM with 5% fetal bovine serum and 1% antibiotic/antimycotic (Gibco, Amarillo, TX).

METHOD DETAILS

Mouse infection with SARS-CoV-2

Male WT B6, K18-hACE2 and IL-33$^{-/-}$ mice (B6 background) were maintained in our animal facility as described above. Animals were anesthetized with isoflurane (1-4%) prior to intranasal infection with either the CMA3p20 strain (5×10^5 PFU for WT B6 mice and IL-33$^{-/-}$ mice) or the Delta strain (1×10^5 PFU for K18-hACE2 mice). Recombinant IL-33 (1 μg/mouse/day) was administered intranasally at day 1 and day 3 post-infection (D1 and D3). Animals were monitored daily for weight loss and morbidity, and were euthanized at D2 and D4 for tissue collection. Mock-treated mice received equal volumes of Vero E6 cell culture medium. All mouse infection studies were performed in the ABSL3 facility in the Galveston National Laboratory located at UTMB; all tissue processing and analysis procedures were performed in BSL3 or BSL2 facilities.

Lung histopathology

Lung tissues were fixed in 10% neutral buffered formalin, embedded in paraffin, sectioned at 5 μm thickness and stained with hematoxylin and eosin for routine histological examination. Slides were examined by a pathologist in a double-blind manner and imaged using an Olympus CX43 microscope. Inflammatory infiltrates and alterations within alveoli, alveolar septa, and airways were assessed.

Viral RNA quantification and qRT-PCR

RNA from lung tissues was collected using RNALater (Qiagen, Hilden, Germany). Samples were subsequently homogenized with Trizol reagent (ThermoFishier Scientific, Waltham, MA) in a BeadBlaster 24 Microtube Homogenizer (Benchmark Scientific, Sayreville, NJ). RNA was then extracted from Trizol using an RNeasy Mini kit (Qiagen, Hilden, Germany) per the manufacturer's instruction. Viral RNA was quantified using an iTaq Universal Probes One-Step kit (Bio-Rad, Hercules, CA) and SARS-CoV-2 qPCR Primer & Probe kit (Integrated DNA Technologies, Coralville, IA). 2019-nCoV_N positive control (2×10^5 copies/mL) and N1 (IBFQ) were used for standard curves and primer/probe, respectively. The results were calculated as copy numbers per nanogram of total tissue RNA. For assessment of lung inflammatory genes, extracted tissue RNA was converted to cDNA with the iScript cDNA Synthesis kit (Bio-Rad, Hercules, CA). cDNA was amplified in a 10 μL reaction mixture containing 5 μL of iTaq SYBR Green Supermix (Bio-Rad, Hercules, CA) and 5 μM each of gene-specific forward and reverse primers. PCR reactions were denatured for 30s at 95°C, followed by 40 cycles of 15s at 95°C, and 60s at 60°C utilizing the CFX96 Touch real-time PCR detection system (Bio-Rad, Hercules, CA). Relative quantitation of mRNA expression was calculated using the $2^{-\Delta\Delta Ct}$ method. The primer sequences are listed in Table S1.

Flow cytometry

Left lung lobes were harvested from mice, minced, and digested with 0.05% collagenase type IV (Thermo Fisher Scientific, Waltham, MA) in RPMI 1640 medium for 30 minutes at 37°C. Minced tissues were loaded into Medicons and homogenized using a BD Mediamachine System (BD Biosciences, Franklin Lakes, NJ). Single-cell suspensions were made by passing cell homogenates through 70-μm cell strainers followed by treatment with a Red Cell Lysis Buffer (Sigma-Aldrich, St. Louis, MO). Leukocytes were stained with the Fixable Viability Dye eFluor 506 (ThermoFisher Scientific, Waltham, MA) for live/dead cell staining, blocked with FcγR, and stained with fluorochrome-labeled antibodies (Abs). The following Abs were purchased from ThermoFisher Scientific and BioLegend: PE-Cy7-anti-CD3ϵ (145-2C11), Pacific Blue-anti-CD4 (GK1.5), APC-efluor780-anti-CD8a (53-6.7), APC-anti-Ly6G (1A8-Ly6G), PE-CF594-anti-NK1.1 (PK136), FITC-anti-CD64 (X54-5/7.1), Alexafluor700-anti-CD11b (M1/70), BV711-anti-CD44 (IM7), APC-anti-gd TCR (GL3), PE-anti-CD45 (30-F11) and FITC-anti-CD69 (H1.2F3). Cells were fixed in 2% paraformaldehyde overnight at 4°C before analysis. Data were collected using a BD LSR Fortessa and analyzed via FlowJo software version 10 (BD Bioscience, Franklin Lakes, NJ).

Western blot analysis

Lung tissues were homogenized in RIPA buffer containing 1% protease inhibitor cocktail (Sigma-Aldrich, St. Louis, MO). Protein concentration was determined by Pierce™ BCA Protein Assay Kit (ThermoFisher Scientific, Waltham, MA). Western blot analysis was performed to analyze IL-33 protein levels. Briefly, 20 μg protein per lane was loaded onto 4–15% Tris-glycine gradient gel (ThermoFisher Scientific, Waltham, MA). Samples were transferred to PVDF membrane and blotted with IL-33 (#ab187060, Abcam, Cambridge, United Kingdom) and β-actin (#4967, Cell Signaling Technology, Danvers, MA) primary antibodies at 4°C overnight. Antibody detection was accomplished using horseradish peroxidase conjugated secondary antibodies and visualized with ECL. The signal intensity was quantified with Image J.

Collection of plasma and nasopharyngeal swab samples from COVID-19 patients

Plasma and nasopharyngeal swab samples were collected from patients that were diagnosed with COVID-19 and admitted to a UTMB hospital between March 2020 and March 2021 (Table S2). Patients were categorized into four groups based on their oxygen therapy requirements. 1) Mild disease group: Patients not needing oxygen therapy; 2) Moderate disease group: Patients requiring oxygen via nasal cannula; 3) Severe disease group: Patients needing non-invasive ventilation methods like high-flow nasal cannula, CPAP, BiPAP, or venturi mask; and 4) Critical disease group: Patients requiring invasive mechanical ventilation or extracorporeal membrane oxygenation (ECMO). SARS-CoV-2 infection was confirmed in all subjects either through reverse transcriptase-polymerase chain reaction (RT-PCR) or through detection of viral antigens in the samples. Clinical and laboratory data for patients diagnosed with COVID-19 were obtained from the medical record. Plasma and nasopharyngeal swab samples were collected from 61 patients of varying disease severity and stored at the UTMB Biorepository for Severe Emerging Infections at -80°C until use. Plasma and nasopharyngeal swab samples were also collected from twenty healthy individuals who tested negative for SARS-CoV-2 and did not have any underlying health conditions. Plasma samples were collected from anticoagulant-treated whole blood after centrifugation at 1,200 g for 10 minutes at 4°C. All samples were inactivated either by heating at 56°C for 30 minutes or γ-irradiated and validated before transfer outside of BSL3.

Human IL-33 ELISA assay

IL-33 levels in patient samples were quantified using a Human IL-33 Quantikine ELISA Kit (R&D, Minneapolis, MN) according to the manufacturer's instruction. The assay range of the kit is 3.1 - 200 pg/mL. The sensitivity is 1.5 pg/mL. Samples with undetectable IL-33 levels were excluded from the analysis.

Multiplex cytokine/chemokine analysis

Mouse sera were separated using a Microtainer Tube with Serum Separator (BD Biosciences, Franklin Lakes, NJ) and inactivated at 56°C for 30 minutes. Serum cytokine/chemokine concentrations were determined using a Bio-Plex Pro Mouse Cytokine 23-plex Assay kit (Bio-Rad, Hercules, CA) according to manufacturer's protocol. Samples were read by a Bio-Plex 200 system (Bio-Rad, Hercules, CA), and the calculation of both absolute concentrations and relative fold changes were performed.

Lung tissue RNA-seq assay

RNA-seq analysis was performed by LC Sciences (Houston, TX) and RNA purity/quantity was assessed using a Bioanalyzer 2100 and RNA 6000 Nano LabChip Kit (Agilent Technologies, Santa Clara, CA). Extraction of mRNA, construction of cDNA libraries, and sequencing were performed using the Illumina Novaseq 6000. Raw data were normalized and analyzed by ROSALIND (San Diego, CA). The Mus musculus genome build mm10 was used as a reference genome. Quality control analysis was done using FastQC and RSeQC6.[42] ROSALIND used HTseq4 to quantify individual sample reads and DESeq2 R library to normalize reads via Relative Log Expression.[43,44] Enrichment was determined by hypergeometric distribution and was calculated relative to a background gene set that was relevant for the experiment. The Molecular Signatures Database was referenced for collection of "hallmark" gene sets. The RNA-seq data presented herein were deposited in NCBI's Gene Expression Omnibus and is accessible through GEO Series accession number GSE247370.

Ingenuity pathway analysis

RNA-seq data were analyzed using Qiagen Ingenuity Pathway Analysis (IPA). Canonical pathways analysis identified the most significant pathways from the Qiagen IPA library that were relevant to the dataset. Molecules that met the following criteria of fold changes with a cutoff of 1.5 and adjusted *p*-value of 0.05 and associated with a canonical pathway in the Qiagen Knowledge Base were included in the analysis. For the pathway network of IL-33 and COVID-19, both "Infectious Diseases" and "Organismal Injury and Abnormalities" were selected for analysis. The comparison analysis was performed based on the results of the IPA core analysis.

QUANTIFICATION AND STATISTICAL ANALYSIS

Data are presented as mean ± standard deviation (SD). An unpaired/two-tailed t test was employed to compare two groups. Datasets with more than two groups were analyzed using a one-way ANOVA followed by Tukey's multiple comparisons test for pairwise comparisons. Body-weight changes were analyzed by repeated measured two-way ANOVA with group (between factor), time (within factor) and group by time interaction. After a significant interaction test, pairwise comparisons were performed by Tukey's multiple comparisons test at each time point. All data were analyzed by using GraphPad Prism software 10 (GraphPad, La Jolla, CA, USA). All p-values are adjusted by multiple comparisons. All tests are two-sided with a significance level of 0.05. Statistically significant values are denoted with asterisks with * $p < 0.05$, ** $p < 0.01$, *** $p < 0.001$, and **** $p < 0.0001$, respectively. Only statistically significant comparisons are shown.